PLOS | ONE

RESEARCH ARTICLE

Crystal Structure of DIM-1, an Acquired Subclass B1 Metallo-β-Lactamase from *Pseudomonas stutzeri*

Michael P. S. Booth[1], Magda Kosmopoulou[1], Laurent Poirel[2], Patrice Nordmann[2], James Spencer[1]*

1 School of Cellular and Molecular Medicine, University of Bristol Medical Sciences Building, University Walk, Bristol, BS8 1TD, United Kingdom, **2** Medical and Molecular Microbiology Unit, Department of Medicine, Faculty of Science, University of Fribourg, Rue Albert Gockel 3, CH-1700, Fribourg, Switzerland

* Jim.Spencer@bristol.ac.uk

Citation: Booth MPS, Kosmopoulou M, Poirel L, Nordmann P, Spencer J (2015) Crystal Structure of DIM-1, an Acquired Subclass B1 Metallo-β-Lactamase from *Pseudomonas stutzeri*. PLoS ONE 10(10): e0140059. doi:10.1371/journal.pone.0140059

Editor: Anna Roujeinikova, Monash University, AUSTRALIA

Received: April 22, 2015

Accepted: September 20, 2015

Published: October 9, 2015

Data Availability Statement: Crystal structures (co-ordinates and structure factors) have been deposited in the Protein Data Bank (www.rcsb.org/pdb) with accession codes 4WD6 and 4ZEJ.

Funding: This study was supported by the British Society for Antimicrobial Chemotherapy (www.bsac.org; grant no. GA820 to J.S.), the U.K. Medical Research Council (www.mrc.ac.uk; grant no. G1100135 to J.S.), and the U.S. National Institutes of Allergy and Infectious Disease (http://www.niaid.nih.gov/; grant no. 1R01AI100560-01 to J.S.). The funders had no role in study design, data collection

Abstract

Metallo-β-lactamases (MBLs) hydrolyze almost all classes of β-lactam antibiotic, including carbapenems—currently first choice drugs for opportunistic infections by Gram-negative bacterial pathogens. MBL inhibitor development is complicated by the diversity within this group of enzymes, and by the appearance of new enzymes that continue to be identified both as chromosomal genes and on mobile genetic elements. One such newly discovered MBL is DIM-1, a mobile enzyme originally discovered in the opportunist pathogen *Pseudomonas stutzeri* but subsequently identified in other species and locations. DIM-1 is a subclass B1 MBL more closely related to the TMB-1, GIM-1 and IMP enzymes than to other clinically encountered MBLs such as VIM and NDM; and possesses Arg, rather than the more usual Lys, at position 224 in the putative substrate binding site. Here we report the crystallization and structure determination of DIM-1. DIM-1 possesses a binuclear metal center with a 5 (rather than the more usual 4) co-ordinate tri-histidine (Zn1) site and both 4- and 5-co-ordinate Cys-His-Asp- (Zn2) sites observed in the two molecules of the crystallographic asymmetric unit. These data indicate a degree of variability in metal co-ordination geometry in the DIM-1 active site, as well as facilitating inclusion of DIM-1 in structure-based MBL inhibitor discovery programmes.

Introduction

Acquired metallo-β-lactamases (MBLs) present a global public health challenge [1]. Their high hydrolytic activity against carbapenems, (broad-spectrum β-lactams of ultimate choice for Gram-negative infections), and their non-susceptibility to serine β-lactamase inhibitors, make their dissemination significant in the rise of antibiotic resistant pathogens. Sequence data define three MBL subclasses (B1 –B3 [2]) with B1 including almost all enzymes whose genes are found on mobile genetic elements, and thus capable of rapid dissemination across geographic and species boundaries. B1 MBLs from the IMP, VIM and NDM groups have already been found in

and analysis, decision to publish, or preparation of the manuscript.

Competing Interests: The authors have declared that no competing interests exist.

multiple hosts, both Enterobacteriaceae [3] and non-fermenters (*Pseudomonas aeruginosa*, *Acinetobacter baumannii* [4–6]), while additional mobile enzymes [7–9] continue to be identified.

DIM-1 (Dutch IMipenemase) was identified in a carbapenem non-susceptible isolate of the occasional opportunist pathogen *Pseudomonas stutzeri*, recovered from a patient undergoing surgery for tibial osteomyelitis [10]. The carbapenemase gene, bla_{DIM-1} (GenBank: GU323019.1), resided on a class 1 integron on a 70 kb plasmid, suggesting a capability for dissemination, and has subsequently been identified in isolates of multiple species (*Escherichia coli*, *Enterobacter cloacae*, *Comomonas testosteroni*) of African origin and in a single strain of *P. stutzeri* from India [11, 12]. Independent acquisition events from a currently unknown environmental reservoir have been suggested to account for these apparently unconnected identifications in widely separated locations [11]. The bla_{DIM-1} gene encodes a subclass B1 MBL resembling TMB-1 (67% identity [7]) GIM-1 (54% identity [13]) and IMP-1 (48% identity [14]; percentage identities are for the mature, processed polypeptides), but more distantly related to VIM-1 and NDM-1. An alignment of selected B1 MBLs is presented in Fig 1.

Like other B1 MBLs, DIM-1 is a broad-spectrum enzyme, hydrolyzing penicillins, cephalosporins and carbapenems, although compared to some enzymes turnover of some penicillins is reduced and activity is weaker against cephalosporins, e.g. ceftazidime or cefepime, with bulky, charged, 3' substituents [10]. In common with GIM-1 and TMB-1, DIM-1 is distinguished from other B1 enzymes by possession of arginine at position 224, rather than the lysine (Lys224) found in enzymes such as the IMP and NDM groups. Recent crystal structures [16, 17] show NDM-1 Lys224 to make electrostatic interactions with the C3 carboxylate of hydrolyzed carbapenems, suggesting that this substitution might affect substrate binding. Here we report the crystal structure of DIM-1, facilitating its inclusion in structure-based inhibitor discovery programmes.

Materials and Methods

Protein Expression

DIM-1 was purified from *E. coli* TOP10 containing the plasmid pXD-1 [10] by ion-exchange and size exclusion chromatography in a modification of previously published procedures. Briefly, 2 L of Luria-Bertani broth were inoculated with 10 mL / L of an overnight culture and grown for 24 h at 37°C with shaking at 160 rpm. Cells were harvested by centrifugation (4 000 g, 20 min, 4°C), washed in phosphate-buffered saline (PBS) and frozen until required. Thawed pellets were resuspended in 25 mL / L Buffer A (50 mM Tris-Cl pH 7.5) containing protease inhibitors (Complete EDTA-free, Roche Life Science, Burgess Hill, U.K.) and lysed by sonication. The lysate was clarified by centrifugation (15,000 g, 30 min, 4°C) and dialyzed overnight (4°C) against 1 L buffer A. The dialysate was loaded onto a 50 mL Q-sepharose column (Sigma, Poole, U.K.) which was washed in buffer A until absorbance returned to baseline. Bound protein was eluted in buffer A using a 300 mL 0–0.5 M NaCl gradient; DIM-1 eluted at approximately 0.1 M NaCl as identified by hydrolysis of the chromogenic cephalosporin nitrocefin [18]. DIM-1 containing fractions were concentrated by centrifugal ultrafiltration, loaded onto a 300 mL Superdex-75 column pre-equilibrated in Buffer B (50 mM Tris-Cl 200 mM NaCl pH 7.5) and eluted in the same buffer. The purity of the final preparation was greater than 95% as adjudged by SDS—PAGE [19]. The purified protein was concentrated for crystallization trials by centrifugal ultrafiltration.

Crystallization and Structure Solution

Sparse matrix crystallization screening with the Morpheus suite [20] used a Pheonix robot (Art-Robbins) to set sitting drops (0.5 μL each of DIM-1 (15 mg / mL) and reservoir solution)

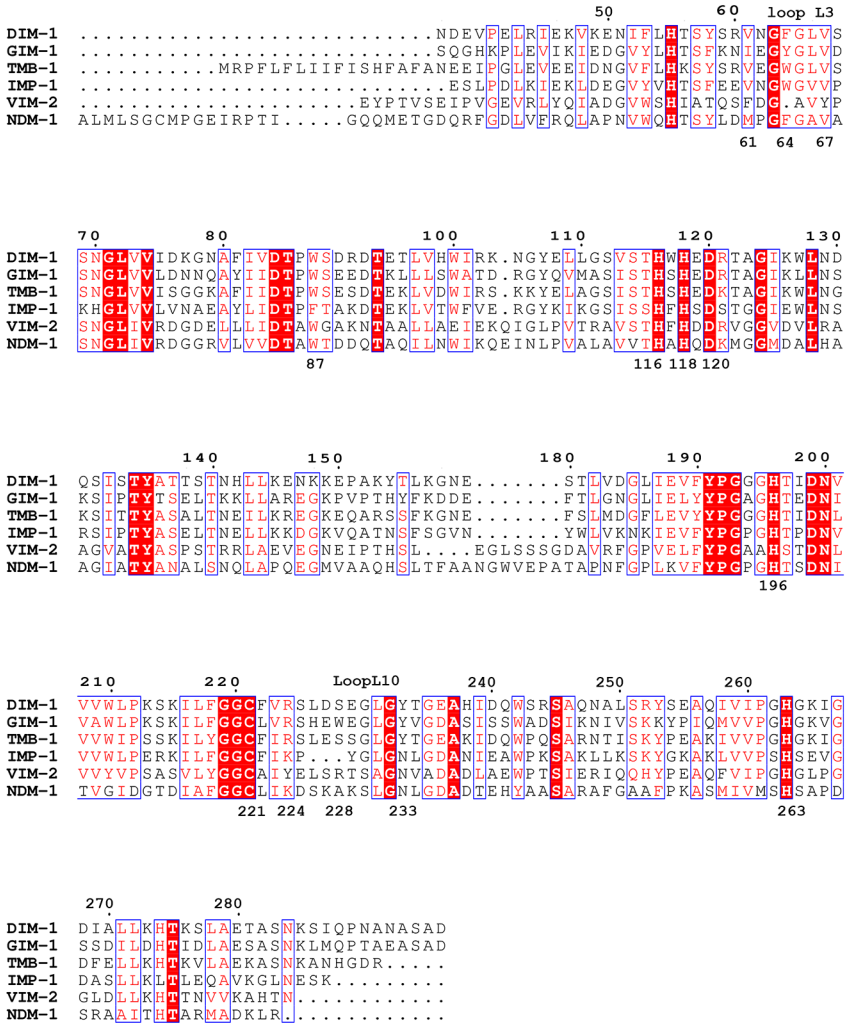

Fig 1. Alignment of DIM-1 with Selected Subclass B1 Metallo-β-Lactamases. Invariant residues are highlighted on a red background; conservative substitutions are colored red. Residue numbers according to the Class B β-Lactamase (BBL) standard numbering scheme are positioned above the sequences; individual residues discussed in the text are numbered below the sequences. This Figure was prepared using ESPript [15].

doi:10.1371/journal.pone.0140059.g001

in 96-well plates with 100 μL well volume. Crystals appeared after 5–10 days' incubation (20°C) in 20% polyethylene glycol (PEG) 550 monomethyl ether (MME) / 10% PEG 20 000; 50 mM HEPES / 50 mM MOPS pH 7.5; were mounted in rayon loops, snap-frozen and stored in liquid nitrogen until required. For soaking experiments, ceftazidime (Sigma, Poole, U.K.) dissolved to 250 mM in dimethyl sulfoxide (DMSO) was added to the drop to a final concentration of 85 mM and 33% DMSO and crystals frozen after 1 hour incubation at 20°C. Diffraction data were collected on an ADSC Quantum 4 detector mounted on beamline I03 of Diamond Light Source (Didcot, U.K.) and reflections integrated, scaled and merged using HKL2000 [21]. Phases were obtained by molecular replacement using PHASER [22] with IMP-1 (PDB accession 1DDK; [23]) as a search model. The model was built using Coot [24] and refined using Refmac5 [25] as implemented in the CCP4 software suite [26] with TLS (Translation/Libration/Screw) groups identified by the TLSMD server [27, 28]. The quality of the final model was assessed using PROCHECK [29] and Molprobity [30]. Data collection and refinement statistics

are given in Table 1. Co-ordinates and structure factors have been deposited with the Protein Data Bak (www.rcsb.org) with accession codes 4WD6 (native structure) and 4ZEJ (ceftazidime-exposed structure).

Results and Discussion

DIM-1 crystallized in space group P 2_1 2_1 2_1 with crystals containing two molecules in the asymmetric unit (Table 1). The structure was solved by molecular replacement and could be built as two polypeptide chains. Two complete data sets were collected, a native data set from a crystal diffracting to 2.2 Å resolution (dataset 1) and a second, higher resolution data set (dataset 2) arising from one of a number of crystals that had been soaked with the cephalosporin ceftazidime in DMSO, but for which no electron density corresponding to a bound β-lactam could be resolved. As this crystal diffracted to higher resolution (1.8 Å) and yielded higher quality data (Table 1) this structure was also solved and refined. Non-crystallographic symmetry was not employed at any stage in the refinement process; therefore our data provide structures for four independently refined DIM-1 monomers. The final models contain 219 (residues

Table 1. Data Collection and Refinement Statistics.

Dataset	Dataset 1	Dataset 2
Processing	HKL2000 [21]	HKL2000
Beamline	DLS I03	DLS I03
Space Group	P 2_1 2_1 2_1	P 2_1 2_1 2_1
Cell Dimensions (Å)	a = 47.72 b = 47.86 c = 185.22	a = 46.40 b = 46.98 c = 183.76
Wavelength (Å)	0.9763	0.9763
Resolution (Å)	50.00–2.20 (2.28–2.20)[a]	50.00–1.80 (1.86–1.80)[a]
Total reflections	149 531	496 348
Unique reflections	21 133 (1 504)[a]	38 481 (3 667)[a]
Completeness (%)	94.5 (68.4)[a]	99.6 (96.6)[a]
Redundancy	7.1 (5.9)[a]	12.9 (7.0)[a]
I / (sig. I)	32.5 (6.6)[a]	29.6 (2.5)[a]
R_{merge} (%)	5.1 (25.1)[a]	8.8 (50.1)[a]
Refinement	REFMAC5	REFMAC5
Total reflections	20 006 (1 016)[a]	36 522 (2 499)[a]
Resolution (Å)	42.55–2.20 (2.26–2.20)[a]	91.88–1.79 (1.84–1.79)[a]
R_{cryst} (%)	20.7 (23.9)[a]	17.2 (21.7)[a]
R_{free} (%)[b]	27.4 (34.2)[a]	18.9 (22.8)[a]
RMS bond length (Å)	0.0138	0.0078
RMS bond angle (Å)	1.6167	1.2289
Protein atoms	3 392	3 434
Water molecules	126	192
% residues in Ramachandran regions (favored/ allowed/disallowed)	95.3/4.2/0.5	97.2/2.3/0.5
B-factors (protein)[c]	47.38 (55.26)	30.98 (39.81)
B-factors (water molecules)	48.57	38.68
PDB accession code	4WD6	4ZEJ

[a] Data for the highest resolution shell are in parentheses.

[b] R_{free} was calculated with 5% of the reflections omitted.

[c]Figures in parentheses are for chain B.

doi:10.1371/journal.pone.0140059.t001

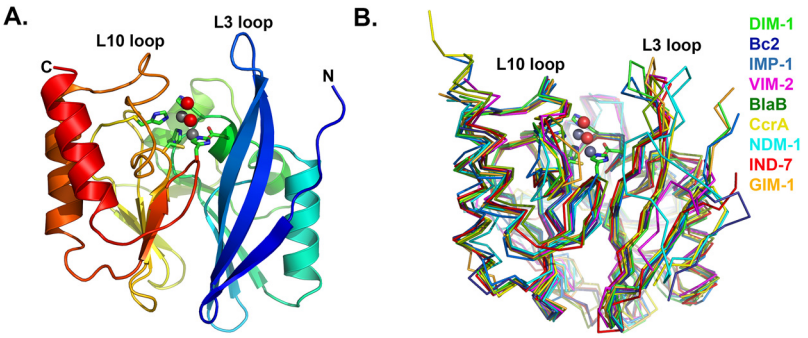

Fig 2. Crystal Structure of DIM-1. A. Overall fold of the enzyme. Protein backbone is color-ramped from blue (N-) to red (C-terminus). Active site residues are rendered as sticks (carbon atoms in green, other atom colors as standard). Zinc ions (gray) and water molecules (red) are shown as spheres. B. Superposition of B1 MBL structures: DIM-1 (green); BcII (pdb accession 1BC2 ([43], blue); IMP-1 (1DDK [23], teal); VIM-2 (1KO3 [44], magenta); BlaB (1M2X [45], dark green); CcrA (1ZNB [46], yellow); NDM-1 (3Q6X [41], cyan); IND-7 (3L6N [47], red) and GIM-1 (2YNT [48], orange). This Figure was generated using Pymol (www.pymol.org).

doi:10.1371/journal.pone.0140059.g002

39–294 according to the standard class B β-lactamase (BBL) numbering scheme [2]) amino acids per chain, apart from chain B of the lower resolution structure (dataset 1) for which weak electron density meant that residues 25–28 (60–64; BBL residue numberings are given in parentheses throughout this paper) inclusive were not modelled. Overall Cα rms deviations between the four chains were a maximum 0.36 Å. For the four chains (A and B of dataset 1 and A and B of dataset 2, respectively) 95/ 94/ 97/ 97% of residues lie within the most favored regions of the Ramachandran plot and a further 4/ 6/ 2/ 2% within the additionally allowed regions [30]. In three of the four chains Asp-48 (84) lies in the disfavored Ramachandran region due to its involvement in a buried hydrogen bond network, involving Ser-33 (69), Asn-34 (70), Thr-76 (115), Arg-82 (121) and Gly-199 (262) that is common to most members of the B1 MBL subfamily and connects the two halves of the protein beneath the active site [31].

DIM-1 adopts the αβ/βα sandwich fold of the MBL hydrolase superfamily, with the active site situated in the groove between the two domains and containing two zinc ions (Fig 2A). Superposition (using SSMsuperpose [32]) with other available B1 MBL structures (Fig 2B) indicates that DIM-1 most closely resembles GIM-1 (Cα rmsd 0.87 Å) and IMP-1 (Cα rmsd 0.91 Å). Among B1 enzymes the MBL fold is well conserved, with significant differences apparent at the N-terminus, in the length of the C-terminal α-helix, and in the flexible loop L3 (residues 25–32 (60–68)) that connects the β2 and β3 strands. Crystallographic [23, 33–35], mutagenic and kinetic [36, 37], NMR [38, 39] and molecular dynamics [40] evidence indicates that this loop adjusts its conformation on β-lactam or inhibitor binding and contributes to substrate affinity and specificity. In the lower resolution (dataset 1) DIM-1 structure the L3 loop could not be modelled for chain B, but in chain A it extends over the active site groove in a "closed" conformation more typical of MBL complexes [17, 34, 35, 41] than of other uncomplexed B1 MBL structures. These differences may arise from differences in crystal contacts-while the apex of loop L3 of chain A lies close both to chain B and symmetry related molecules, fewer contacts are made by the equivalent subunit of chain B. In the higher resolution structure obtained from dataset 2, the complete loop L3 could be modeled for both chains, but chain B featured elevated B-factors consistent with a reduced involvement in crystal contacts. Establishing whether the observed conformation of the DIM-1 L3 loop arises primarily from crystal contacts, or indeed reflects that adopted on substrate and/or inhibitor binding, must await determination of structures for the relevant complexes.

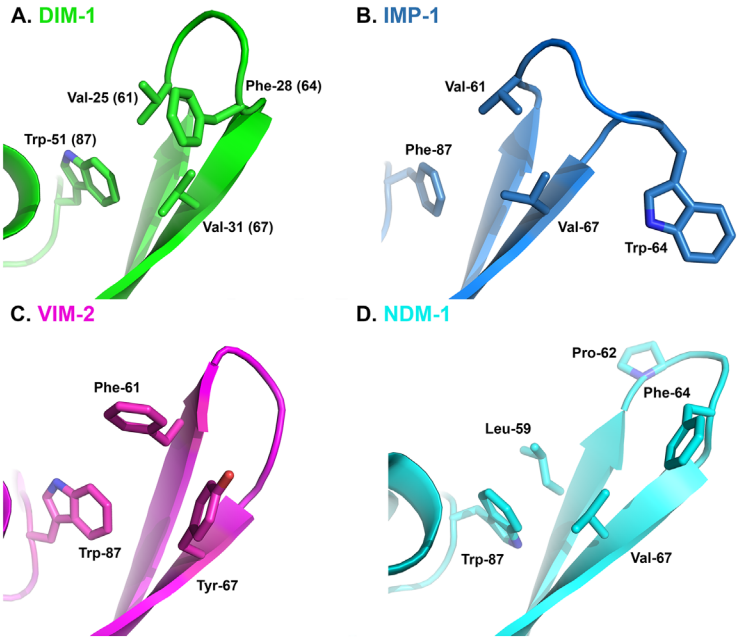

Fig 3. L3 Loop Conformations in Subclass B1 Metallo-β-Lactamases. A. DIM-1 (green); B. IMP-1 (1DDK [23], teal); C. VIM-2 (1KO3 [44], magenta); D. NDM-1 (3Q6X [41], cyan). This Figure was generated using Pymol.

doi:10.1371/journal.pone.0140059.g003

Our structure also confirms that DIM-1 features hydrophobic aliphatic amino acids (valine) at positions 25 (61) and 31 (67) at the base of the L3 loop, and an aromatic residue (phenylalanine) at position 28 (64) at its apex. In this DIM-1 resembles IMP-1 (and similar enzymes such as GIM-1 [13] or KHM-1 [9]) rather than the VIM enzymes (where positions 25 (61) and 31 (67) are occupied by aromatic residues) or NDM-1 (where the L3 loop contains proline at position 26 (62) and adopts a different conformation; Fig 3). As discussed above, inhibitor binding to enzymes such as CcrA [33] or BcII [39] can involve conformational changes in the L3 loop, and be affected by mutations within it [36]. Moreover, comparisons of inhibition of multiple B1 enzymes that differ in their L3 loops (including NDM, IMP and VIM, but not DIM, enzymes) by a series of hydroxythiazole compounds identified differences between enzymes of up to two orders of magnitude in IC_{50} values [42]. Unfortunately, limited structural data are available that permit direct comparison of inhibitor binding to different MBL targets. However, structures for complexes of the thiol L-captopril with IMP-1 (pdb id 4C1F), NDM-1 (pdb 4EXS [17]) and VIM-2 (pdb 4C1D) show that this adopts different conformations that are in part imposed by the proximity of different residues on the L3 loop (residues Met-61 of NDM-1; Val-61 of IMP-1 and Phe-62 and Tyr-67 of VIM-2) to the captopril pyrrolidine ring. Comparison of these structures with that of DIM-1 (Fig 4) suggests that positioning of Phe-28(64) on loop L3 over the active site, together with the presence of Val-25 (61), Val-31 (67) and Trp-51(87) would support an orientation for the binding of the captopril pyrrolidine to DIM-1 that is similar to that adopted upon binding to IMP-1, and that differs from those observed with VIM-2 or NDM-1. It will be of interest to establish the extent to which this similarity between the L3 loops of IMP-1 and DIM-1 results in similar inhibition profiles, and similar modes of inhibitor binding.

Loop L10 (residues 160–176 (223–239)) on the opposite side of the active site groove also shows features that distinguish DIM-1 from related enzymes. The DIM-1 L10 loop lacks Trp-

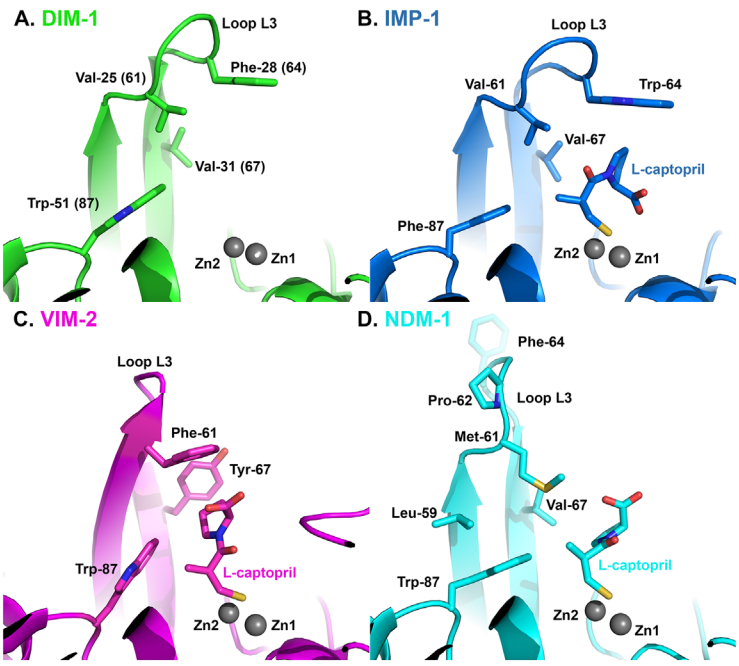

Fig 4. Comparison of DIM-1 Active Site with L-Captopril-bound Complexes of Subclass B1 Metallo-β-Lactamases. A. DIM-1 (green); B. IMP-1 (4C1F, teal); C. VIM-2 (4C1D, magenta); D. NDM-1 (4EXS [17], cyan). This Figure was generated using Pymol.

doi:10.1371/journal.pone.0140059.g004

165 (228), which in GIM-1 restricts this part of the active site cavity [48] and instead has serine at this position. Like GIM-1, DIM-1 possesses tyrosine, rather than the more usual asparagine, at position 170 (233), which further constrains the active site groove and provides a hydrophobic surface for substrate interactions, but abolishes the possible electrostatic contacts between substrate and the Asn-170 (233) side chain that have been proposed for some other B1 enzymes ([17, 35, 49]. The DIM-1 active site also features a close electrostatic contact between the side chains of Glu-78 (119) and Lys-111 (165), forming a bridge across the active site groove in the vicinity of the probable binding site for substituent groups at the R1 position of the β-lactam core (i.e. the C6/C7 substituents of penicillins or cephalosporins, respectively). Taken together, these factors create an active site in DIM-1 that is narrower and more defined than the relatively wide open groove of many other B1 MBLs (Fig 5).

Electron density maps (Fig 6A) unequivocally identify two metal ions in the DIM-1 active site, consistent with the binuclear species being the physiological form of B1 MBLs [51, 52]. As no particular precautions were taken to avoid oxidation of the ligand Cys-158 (221), which is associated with loss of the metal ion in the Zn2 site in certain B1 MBLs, we surmise that this occurs less readily in DIM-1 than in some other enzymes such as BcII, SPM-1 or VIM-2 [31, 45]. All active site metal ions were refined as zinc, with occupancies of 1.0. This procedure yielded B-factors for the individual zinc ions of 42.58 and 48.04 $Å^2$ (chain A Zn1 and Zn2 respectively, dataset 1); 50.73 and 57.25 $Å^2$ (chain B Zn1 and Zn2 respectively, dataset 1); 23.43 and 26.41 $Å^2$ (chain A Zn1 and Zn2 respectively, dataset 2); and 27.13 and 36.58 $Å^2$ (chain B Zn1 and Zn2 respectively, dataset 2). This compares with B-factors for the complete individual protein chains of 47.38 and 55.26 $Å^2$ (chains A and B; dataset 1) and 30.98 and 39.81 $Å^2$ (chains A and B; dataset 2). The consistency between the B-values obtained for the modelled zinc ions and the respective protein chains suggests that refining the bound metal ions as zinc is reasonable. However, while we consider zinc to be the most likely metal ion to be present in the DIM-

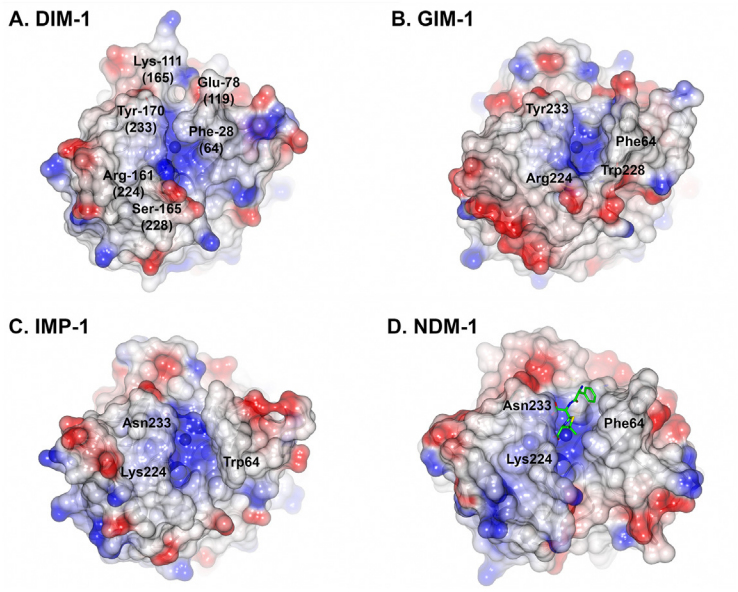

Fig 5. Active Site Grooves of B1 Metallo-β-Lactamases. Figure shows surfaces of A. DIM-1; B. GIM-1 (pdb accession 2YNT [48]) C. IMP-1 (1DDK [23]) and D. NDM-1 (3Q6X [41]) colored according to electrostatic potential from red (- 0.5 V) to blue (+ 0.5 V). Hydrolyzed ampicillin bound to NDM-1 is shown as sticks (carbon atoms green, other atom colors as standard). This Figure was generated using CCP4MG [50].

doi:10.1371/journal.pone.0140059.g005

1 active site, the available data cannot preclude the possibility that some fraction of other metallated species may be present.

In the four independently refined DIM-1 chains the two metal ions lie approximately 4.00 Å–4.40 Å apart (distances in Table 2) and are liganded by the conserved residues His-77 (116), His-79 (118) and His-139 (196) (tri-histidine or Zn1 site); and Asp-81 (120), Cys-158 (221) and His-200 (263); Cys-His-Asp or Zn2 site). A "bridging" water molecule (or hydroxide ion) that is generally proposed to be the nucleophile in the hydrolytic reaction [53], is positioned between the two metal ions (Fig 6A, Wat1), lying closer to Zn1 that Zn2. (Zinc:ligand distances are given in Table 2). (In chain A of the higher resolution structure (dataset 2) this "bridging" ligand was modelled as a chloride ion (chloride was present in the buffer used for size exclusion chromatography)). These features are largely typical of available crystal structures for binuclear B1 MBLs.

B1 MBLs of known structure show a variety of co-ordination geometries at both the Zn1 and Zn2 sites. In the majority of structures the Zn1 site is tetrahedral [46, 48, 54]. However, in three of the four refined active sites DIM-1 contains a pentaco-ordinate Zn1 center with a second water molecule (Fig 6A, Wat2) acting as an additional ligand but at a distance (~2.4–2.5 Å from Zn1) and with elevated B-factors (where both Wat1 and Wat2 are present (dataset 1) Wat2 B-factors 44.31 $Å^2$ and 46.13 $Å^2$ compared to Wat1 B-factors 34.26 $Å^2$ and 39.77 $Å^2$ in chains A and B, respectively) indicative of weaker binding. In the remaining molecule (chain B of dataset 2) this water molecule is absent and the Zn1 site is clearly tetrahedral. The Zn2 site also differs between the four molecules. In the lower resolution structure (dataset 1) this is clearly tetrahedral (four co-ordinate) in molecule A, while in molecule B a second, "apical" water molecule (Fig 6A, Wat3) is present, as observed in other MBL structures [43, 46, 55], to create a pentaco-ordinate center. In the higher resolution structure solved from dataset 2 the position of Wat3 is occupied by chloride ions in both chains, and in both cases Zn2 is five co-ordinated (Fig 6B).

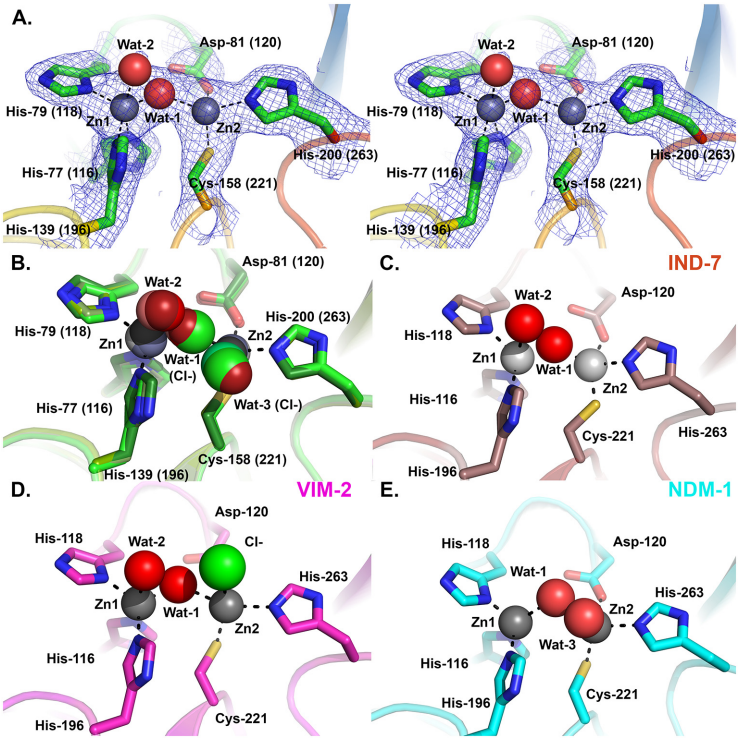

Fig 6. DIM-1 Active Site and Comparison with Selected B1 Metallo-β-Lactamases. A. Stereogram of DIM-1 active site (dataset 1 structure). Carbon atoms are colored green, zinc ions gray, water molecules red, other atom colors as standard. Electron density map shown is 2|Fo|-|Fc|.ϕ_{calc}, contoured at 1.0 σ. B. Overlay of DIM-1 active sites for the four independently refined molecules. Structures from dataset 1 are in darker, and dataset 2 in lighter, shades. Dashed lines show metal:ligand interactions in chain A of dataset 1. Note presence of additional water molecule (Wat-3; dataset 1 chain B) or chloride ions (dataset 2 structures) bound to Zn2 ion, and bridging chloride ion in dataset 2 chain A structure. C. Active site of IND-7 (3L6N [47]). Note five- and four-fold co-ordination of Zn1 and Zn2, respectively. D. Active site of VIM-2 (1KO3 [44]). Not five-fold co-ordination of both Zn^{2+} ions. E. Active site of NDM-1 (3PSU [54]) Note four- and five-fold co-ordination of Zn1 and Zn2, respectively. This Figure was generated using Pymol.

doi:10.1371/journal.pone.0140059.g006

Five co-ordinate Zn1 sites have been observed in some other B1 MBL crystal structures, notably those of IND-7 (Fig 6C, [47]) and reduced VIM-2 (Fig 6D, [44]). Notably, Yamaguchi *et al* [47] used comparisons with structures of biomimetic copper complexes [56] to describe the co-ordination geometry about IND-7 Zn1. Calculation of the structural parameter τ ((β – α)/60), where angle α refers to His79 (118) ND1—Zn1—His139 (196) NE2 and β to O (Wat2) —Zn1—His77 (116) NE2, can be used to represent the distortion from square to trigonal pyramidal co-ordination geometry. (The value of τ is considered to be 0 for an ideal square pyramid and 1 for an ideal trigonal bipyramid). On this basis the IND-7, reduced VIM-2 and DIM-1 Zn1 sites can all be described as distorted trigonal bipyramidal, with values of τ all above 0.85. In all three structures Wat2 is relatively distant from Zn1 compared to other ligands, consistent with proposals [47] that this defines the position occupied by the carbonyl oxygen of incoming β-lactams and hence may be readily displaced when substrates bind. Superposition with structures of NDM-1 complexes with hydrolysed β-lactams (e.g. 3Q6X; [41] Fig 7) indeed locates DIM-1 Wat-2 in the approximate position of the C7 carboxylate formed on β-lactam hydrolysis and thus supports this assertion.

The structural parameter τ can also be used to describe the geometry of the Zn2 site. As described above, defining angles α as (Wat1 (Cl^-))—Zn2—His200 (263) NE2 and β as O (Wat3

Table 2. Metal:ligand distances (Å).

Structure	Dataset 1	Dataset 2
Zn1:His77(116)	2.35[a] (2.19)[b]	2.16[a] (2.18)[b]
Zn1:His79(118)	2.05 (2.34)	2.05 (2.16)
Zn1:His139(196)	2.12 (2.32)	2.09 (2.07)
Zn1:Wat1	1.81 (1.89)	2.26[c] (1.99)
Zn1:Wat2	2.53 (2.40)	2.52
Zn2:Asp81(120)	2.33 (2.60)	2.03 (2.09)
Zn2:Cys168(221)	2.16 (2.11)	2.19 (2.13)
Zn2:His200(263)	2.24 (2.12)	2.15 (2.20)
Zn2:Wat1	2.44 (2.37)	2.27[c] (2.75)
Zn2:Wat3	(2.43)	2.47[c] (2.87)[c]
Zn1:Zn2	3.97 (4.02)	4.22 (4.39)
Wat-1:Asp81(120)	2.94 (3.24)	2.98 (3.04)

[a]Chain A.

[b]Figures in parentheses are for chain B.

[c]Refined as a chloride ion

doi:10.1371/journal.pone.0140059.t002

(Cl^-))—Zn2—Asp81 (120) OD2 gives values of τ ranging from 0.18 to 0.37 for the three chains where Zn2 is five-co-ordinate. This indicates that the DIM-1 Zn2 site can be described as a distorted square pyramid rather than the trigonal bipyramid observed in e.g. VIM-2 (Fig 6D pdb 1KO3 [44]). Under these criteria the Zn2 sites of NDM-1 (Fig 6E, pdb 3SPU [54]) and CcrA

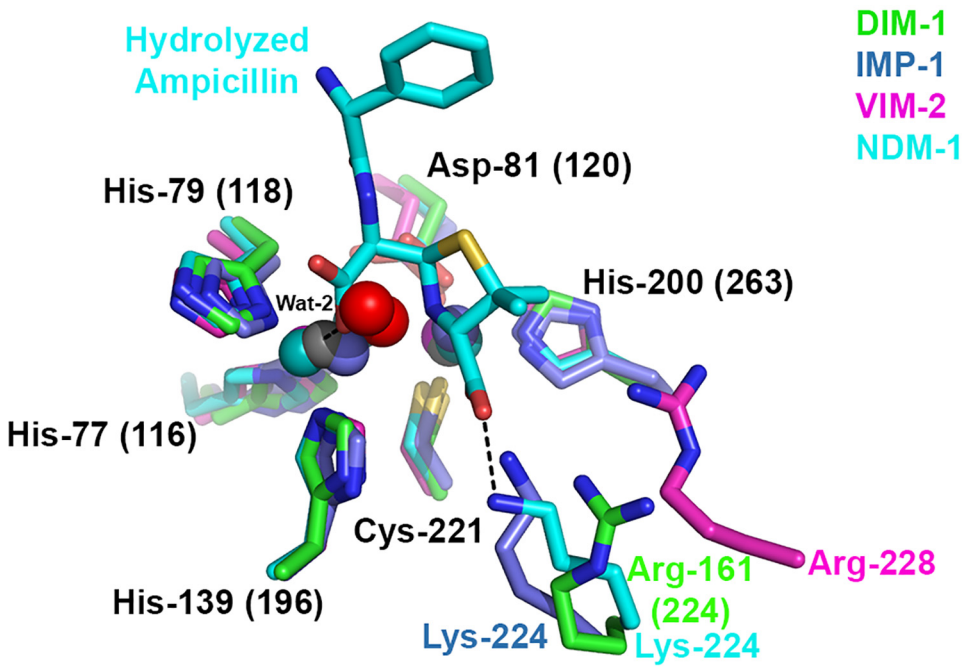

Fig 7. Overlay of B1 Metallo-β-Lactamase Active Sites Showing Hydrolyzed β-Lactam Binding. Figure shows DIM-1, IMP-1 (1DDK [23], carbon, zinc and waters teal); VIM-2 (1KO3 [44], carbon, zinc and waters magenta) and NDM-1:ampicillin complex (3Q6X [41], carbon, zinc and waters cyan). Interactions of hydrolyzed ampicillin with NDM-1 are shown as dashed lines. Note differing positions of Arg-161 (224) (DIM-1), Lys-224 (IMP-1, NDM-1) and Arg-228 (VIM-2). This Figure was generated using Pymol.

doi:10.1371/journal.pone.0140059.g007

(pdb 1ZNB [46]) can also be described as square pyramidal. An additional contrast is provided by the IND-7 (Fig 6C [47]) and GIM-1 [48] structures, where in both cases Zn2 is tetrahedrally co-ordinated, as observed in one of the four DIM-1 chains described here.

The separation of the two active site metal ions in the four DIM-1 structures ranges from 3.97 Å (dataset 1 chain A) to 4.39 Å (dataset 2 chain B). While comparison with other structures is complicated by the lack of atomic resolution data (overall coordinate errors based on R-values are 0.36 Å, dataset 1, and 0.13 Å, dataset 2), these values appear to be at the upper end of the range observed in other B1 MBL structures, which for uncomplexed enzymes lies more typically in the 3.5–3.7 Å range (e.g. IND-7 3.64 Å, pdb 3L6N [47]; GIM-1 3.45–3.50 Å pdbs 2YNT and 2YNW [48]) and see recent near-atomic resolution structures of BcII (3.50 Å, 1.20 Å resolution, pdb id 4C09) and VIM-2 (3.51 Å, 1.29 Å resolution, pdb id 4BZ3). Increased separations have been observed for structures determined under more acidic conditions [16, 57], and the metal—metal distance is also observed to increase in some complexes with hydrolyzed β-lactams (e.g. NDM-1:ampicillin pdb 3Q6X 4.58 Å [41] compared to unliganded NDM-1 3.56–3.97 Å pdb 3SPU), indicating that the MBL active site architecture is able to adapt to accommodate bound ligands. It is notable that other structures in which, as is the case for dataset 2, chloride ions are observed in the MBL active site (e.g. 1KO3 [44] or 2BG2 [57]) also feature relatively large separations between the two zinc ions (4.20 Å and 4.09 Å respectively). Our observation of a variety of metal co-ordination arrangements in DIM-1, and the range of architectures observed in the zinc sites of other enzymes, together highlight the flexibility of co-ordination geometry about both metal ions of the B1 MBL active site (for a review see [58]). This is also consistent with proposals that metal co-ordination geometry can change during β-lactam binding and hydrolysis [59–61].

In common with some other mobile B1 MBLs (e.g. GIM-1 and TMB-1; [7, 13]) DIM-1 features an arginine at residue 161 (224), rather than the lysine found at the equivalent position in most other enzymes (e.g. NDM-1, IMP-1, SPM-1, IND-7). Structures of inhibitor and β-lactam complexes of the IMP-1 and NDM-1 enzymes [17, 23, 41], as well as evidence from directed mutagenesis studies [62, 63], implicate this lysine in substrate interactions via the invariant carboxylate at the β-lactam C3 (penicillin) or C4 (cephalosporin) position. Structural comparisons (Fig 7) suggest that DIM-1 Arg161 (224) NH1 might make similar contacts, although we note that, relative to Zn2 (also implicated in binding substrate carboxylate) DIM-1 Arg161 (224) NH1 is not identically located to Lys224 NZ of e.g. IMP-1 or NDM-1. Steady-state kinetic data [7, 10, 13] show enzymes with Arg224 to be less efficient than other B1 MBLs against some substrates, in particular penicillins (for which k_{cat} values are notably reduced [7]). It is possible that interactions involving Arg224, rather than Lys224, result in binding of some substrates in orientations that are less optimal for hydrolysis.

In summary, the DIM-1 crystal structure presented here displays similarities and differences when compared to those for other B1 MBLs. While the overall fold and binuclear zinc center are common to all B1 MBLs, the DIM-1 structure highlights the variability evident in the active site architecture around the L3 and L10 loops and in the identity and location of residues (DIM-1 Arg161 (224)) likely to be involved in binding the β-lactam C2/C3 carboxylate. Moreover, our data provide further evidence of variability in the co-ordination of both of the catalytic zinc ions in B1 MBLs. Possession of a relatively plastic active site which differs significantly between individual enzymes is one reason why MBLs remain challenging targets for inhibitor design. The availability of structural information for enzymes, such as DIM-1, whose active sites contain such distinguishing features and that, by virtue of their mobilization and presence in pathogens, are a present challenge to clinical β-lactam use, is thus a stepping stone to development of broad spectrum inhibitors effective across the full range of MBLs.

Acknowledgments

We thank Diamond Light Source for access to beamline I03 (proposal number MX313) that contributed to the results presented here, and Philip Hinchliffe, Ramya Salimraj and Martin Challand for their careful reading of the manuscript.

Author Contributions

Conceived and designed the experiments: MPSB JS. Performed the experiments: MPSB. Analyzed the data: MPSB MK JS. Contributed reagents/materials/analysis tools: LP PN. Wrote the paper: JS.

References

1. Cornaglia G, Giamarellou H, Rossolini GM. Metallo-beta-lactamases: a last frontier for beta-lactams? The Lancet infectious diseases. 2011; 11(5):381–93. doi: 10.1016/S1473-3099(11)70056-1 PMID: 21530894.
2. Galleni M, Lamotte-Brasseur J, Rossolini GM, Spencer J, Dideberg O, Frere JM. Standard numbering scheme for class B beta-lactamases. Antimicrob Agents Chemother. 2001; 45(3):660–3. PMID: 11181339.
3. Nordmann P, Naas T, Poirel L. Global spread of Carbapenemase-producing Enterobacteriaceae. Emerg Infect Dis. 2011; 17(10):1791–8. doi: 10.3201/eid1710.110655 PMID: 22000347; PubMed Central PMCID: PMC3310682.
4. Castanheira M, Deshpande LM, Costello A, Davies TA, Jones RN. Epidemiology and carbapenem resistance mechanisms of carbapenem-non-susceptible Pseudomonas aeruginosa collected during 2009–11 in 14 European and Mediterranean countries. J Antimicrob Chemother. 2014. doi: 10.1093/jac/dku048 PMID: 24603963.
5. Edelstein MV, Skleenova EN, Shevchenko OV, D'Souza J W, Tapalski DV, Azizov IS, et al. Spread of extensively resistant VIM-2-positive ST235 Pseudomonas aeruginosa in Belarus, Kazakhstan, and Russia: a longitudinal epidemiological and clinical study. The Lancet infectious diseases. 2013; 13 (10):867–76. Epub 2013/07/13. doi: 10.1016/s1473-3099(13)70168-3 PMID: 23845533.
6. Bonnin RA, Poirel L, Nordmann P. New Delhi metallo-beta-lactamase-producing Acinetobacter baumannii: a novel paradigm for spreading antibiotic resistance genes. Future Microbiol. 2014; 9(1):33–41. doi: 10.2217/fmb.13.69 PMID: 24328379.
7. El Salabi A, Borra PS, Toleman MA, Samuelsen O, Walsh TR. Genetic and biochemical characterization of a novel metallo-beta-lactamase, TMB-1, from an Achromobacter xylosoxidans strain isolated in Tripoli, Libya. Antimicrob Agents Chemother. 2012; 56(5):2241–5. doi: 10.1128/AAC.05640-11 PMID: 22290947; PubMed Central PMCID: PMC3346670.
8. Pollini S, Maradei S, Pecile P, Olivo G, Luzzaro F, Docquier JD, et al. FIM-1, a new acquired metallo-beta-lactamase from a Pseudomonas aeruginosa clinical isolate from Italy. Antimicrob Agents Chemother. 2013; 57(1):410–6. doi: 10.1128/AAC.01953-12 PMID: 23114762; PubMed Central PMCID: PMC3535987.
9. Sekiguchi J, Morita K, Kitao T, Watanabe N, Okazaki M, Miyoshi-Akiyama T, et al. KHM-1, a novel plasmid-mediated metallo-beta-lactamase from a Citrobacter freundii clinical isolate. Antimicrob Agents Chemother. 2008; 52(11):4194–7. doi: 10.1128/AAC.01337-07 PMID: 18765691; PubMed Central PMCID: PMC2573105.
10. Poirel L, Rodriguez-Martinez JM, Al Naiemi N, Debets-Ossenkopp YJ, Nordmann P. Characterization of DIM-1, an integron-encoded metallo-beta-lactamase from a Pseudomonas stutzeri clinical isolate in the Netherlands. Antimicrob Agents Chemother. 2010; 54(6):2420–4. doi: 10.1128/AAC.01456-09 PMID: 20308383; PubMed Central PMCID: PMC2876379.
11. Deshpande LM, Jones RN, Woosley LN, Castanheira M. Retrospective molecular analysis of DIM-1 metallo-beta-lactamase discovered in Pseudomonas stutzeri from India in 2000. Antimicrob Agents Chemother. 2014; 58(1):596–8. doi: 10.1128/AAC.01541-13 PMID: 24145536; PubMed Central PMCID: PMC3910751.
12. Leski TA, Bangura U, Jimmy DH, Ansumana R, Lizewski SE, Li RW, et al. Identification of blaOXA-(5)(1)-like, blaOXA-(5)(8), blaDIM-(1), and blaVIM carbapenemase genes in hospital Enterobacteriaceae isolates from Sierra Leone. J Clin Microbiol. 2013; 51(7):2435–8. doi: 10.1128/JCM.00832-13 PMID: 23658259; PubMed Central PMCID: PMC3697688.

13. Castanheira M, Toleman MA, Jones RN, Schmidt FJ, Walsh TR. Molecular characterization of a beta-lactamase gene, blaGIM-1, encoding a new subclass of metallo-beta-lactamase. Antimicrob Agents Chemother. 2004; 48(12):4654–61. PMID: 15561840.

14. Osano E, Arakawa Y, Wacharotayankun R, Ohta M, Horii T, Ito H, et al. Molecular characterization of an enterobacterial metallo beta-lactamase found in a clinical isolate of Serratia marcescens that shows imipenem resistance. Antimicrob Agents Chemother. 1994; 38(1):71–8. PMID: 8141584.

15. Robert X, Gouet P. Deciphering key features in protein structures with the new ENDscript server. Nucleic Acids Res. 2014; 42(Web Server issue):W320–4. doi: 10.1093/nar/gku316 PMID: 24753421; PubMed Central PMCID: PMC4086106.

16. Kim Y, Cunningham MA, Mire J, Tesar C, Sacchettini J, Joachimiak A. NDM-1, the ultimate promiscuous enzyme: substrate recognition and catalytic mechanism. FASEB J. 2013; 27(5):1917–27. doi: 10.1096/fj.12-224014 PMID: 23363572; PubMed Central PMCID: PMC3633820.

17. King DT, Worrall LJ, Gruninger R, Strynadka NC. New Delhi metallo-beta-lactamase: structural insights into beta-lactam recognition and inhibition. J Am Chem Soc. 2012; 134(28):11362–5. doi: 10.1021/ja303579d PMID: 22713171.

18. O'Callaghan CH, Morris A, Kirby SM, Shingler AH. Novel method for detection of beta-lactamases by using a chromogenic cephalosporin substrate. Antimicrob Agents Chemother. 1972; 1(4):283–8. PMID: 4208895.

19. Laemmli UK. Cleavage of structural proteins during the assembly of the head of bacteriophage T4. Nature. 1970; 227(5259):680–5. PMID: 5432063

20. Gorrec F. The MORPHEUS protein crystallization screen. J Appl Crystallogr. 2009; 42(Pt 6):1035–42. doi: 10.1107/S0021889809042022 PMID: 22477774; PubMed Central PMCID: PMC3246824.

21. Otwinowski Z, Minor W. Processing of X-ray Diffraction Data Collected in Oscillation Mode. Method Enzymol. 1997; 276:307–26.

22. McCoy AJ, Grosse-Kunstleve RW, Adams PD, Winn MD, Storoni LC, Read RJ. Phaser crystallographic software. J Appl Cryst. 2007; 40(4):658–74. doi: 10.1107/S0021889807021206

23. Concha NO, Janson CA, Rowling P, Pearson S, Cheever CA, Clarke BP, et al. Crystal structure of the IMP-1 metallo beta-lactamase from Pseudomonas aeruginosa and its complex with a mercaptocarboxylate inhibitor: binding determinants of a potent, broad-spectrum inhibitor. Biochemistry. 2000; 39 (15):4288–98. PMID: 10757977.

24. Emsley P, Lohkamp B, Scott WG, Cowtan K. Features and development of Coot. Acta Crystallogr D Biol Crystallogr. 2010; 66(4):486–501.

25. Murshudov GN, Vagin AA, Dodson EJ. Refinement of Macromolecular Structures by the Maximum-Likelihood Method. Acta Crystallogr D Biol Crystallogr. 1997; 53(3):240–55.

26. Winn MD, Ballard CC, Cowtan KD, Dodson EJ, Emsley P, Evans PR, et al. Overview of the CCP4 suite and current developments. Acta Crystallogr D Biol Crystallogr. 2011; 67(Pt 4):235–42. doi: 10.1107/S0907444910045749 PMID: 21460441; PubMed Central PMCID: PMC3069738.

27. Painter J, Merritt EA. Optimal description of a protein structure in terms of multiple groups undergoing TLS motion. Acta Crystallogr D Biol Crystallogr. 2006; 62(Pt 4):439–50. doi: 10.1107/S0907444906005270 PMID: 16552146.

28. Painter J, Merritt EA. TLSMD web server for the generation of multi-group TLS models. Journal of Applied Crystallography. 2006; 39:109–11. doi: 10.1107/S0021889805038987 WOS:000234679400018.

29. Laskowski RA, MacArthur MW, Moss DS, Thornton JM. PROCHECK: a program to check the stereochemical quality of protein structures. J Appl Cryst. 1993; 26(2):283–91.

30. Chen VB, Arendall WB 3rd, Headd JJ, Keedy DA, Immormino RM, Kapral GJ, et al. MolProbity: all-atom structure validation for macromolecular crystallography. Acta Crystallogr D Biol Crystallogr. 2010; 66(Pt 1):12–21. Epub 2010/01/09. S0907444909042073 [pii] doi: 10.1107/S0907444909042073 PMID: 20057044; PubMed Central PMCID: PMC2803126.

31. Murphy TA, Catto LE, Halford SE, Hadfield AT, Minor W, Walsh TR, et al. Crystal structure of Pseudomonas aeruginosa SPM-1 provides insights into variable zinc affinity of metallo-beta-lactamases. J Mol Biol. 2006; 357(3):890–903. PMID: 16460758.

32. Krissinel E, Henrick K. Secondary-structure matching (SSM), a new tool for fast protein structure alignment in three dimensions. Acta Crystallogr D Biol Crystallogr. 2004; 60(Pt 12 Pt 1):2256–68. PMID: 15572779.

33. Toney JH, Fitzgerald PM, Grover-Sharma N, Olson SH, May WJ, Sundelof JG, et al. Antibiotic sensitization using biphenyl tetrazoles as potent inhibitors of Bacteroides fragilis metallo-beta-lactamase. Chem Biol. 1998; 5(4):185–96. PMID: 9545432.

34. Toney JH, Hammond GG, Fitzgerald PM, Sharma N, Balkovec JM, Rouen GP, et al. Succinic acids as potent inhibitors of plasmid-borne IMP-1 metallo-beta-lactamase. J Biol Chem. 2001; 276(34):31913–8. PMID: 11390410.

35. Yamaguchi Y, Jin W, Matsunaga K, Ikemizu S, Yamagata Y, Wachino J, et al. Crystallographic investigation of the inhibition mode of a VIM-2 metallo-beta-lactamase from Pseudomonas aeruginosa by a mercaptocarboxylate inhibitor. J Med Chem. 2007; 50(26):6647–53. doi: 10.1021/jm701031n PMID: 18052313.

36. Moali C, Anne C, Lamotte-Brasseur J, Groslambert S, Devreese B, Van Beeumen J, et al. Analysis of the Importance of the Metallo-beta-Lactamase Active Site Loop in Substrate Binding and Catalysis. Chem Biol. 2003; 10(4):319–29. PMID: 12725860.

37. Yang Y, Keeney D, Tang X, Canfield N, Rasmussen BA. Kinetic properties and metal content of the metallo-beta-lactamase CcrA harboring selective amino acid substitutions. J Biol Chem. 1999; 274 (22):15706–11. PMID: 10336469.

38. Scrofani SD, Chung J, Huntley JJ, Benkovic SJ, Wright PE, Dyson HJ. NMR characterization of the metallo-beta-lactamase from Bacteroides fragilis and its interaction with a tight-binding inhibitor: role of an active-site loop. Biochemistry. 1999; 38(44):14507–14. PMID: 10545172.

39. Karsisiotis AI, Damblon CF, Roberts GC. Solution structures of the Bacillus cereus metallo-beta-lactamase BcII and its complex with the broad spectrum inhibitor R-thiomandelic acid. Biochem J. 2013; 456 (3):397–407. doi: 10.1042/BJ20131003 PMID: 24059435; PubMed Central PMCID: PMC3898119.

40. Salsbury FR Jr., Crowley MF, Brooks CL 3rd. Modeling of the metallo-beta-lactamase from B. fragilis: structural and dynamic effects of inhibitor binding. Proteins. 2001; 44(4):448–59. PMID: 11484222.

41. Zhang H, Hao Q. Crystal structure of NDM-1 reveals a common {beta}-lactam hydrolysis mechanism. FASEB J. 2011. doi: 10.1096/fj.11-184036

42. Makena A, van Berkel SS, Lejeune C, Owens RJ, Verma A, Salimraj R, et al. Chromophore-linked substrate (CLS405): probing metallo-beta-lactamase activity and inhibition. ChemMedChem. 2013; 8 (12):1923–9. doi: 10.1002/cmdc.201300350 PMID: 24166830.

43. Fabiane SM, Sohi MK, Wan T, Payne DJ, Bateson JH, Mitchell T, et al. Crystal structure of the zinc-dependent beta-lactamase from Bacillus cereus at 1.9 A resolution: binuclear active site with features of a mononuclear enzyme. Biochemistry. 1998; 37(36):12404–11. PMID: 9730812.

44. Garcia-Saez I, Docquier J-D, Rossolini GM, Dideberg O. The three-dimensional structure of VIM-2, a Zn-beta-lactamase from Pseudomonas aeruginosa in its reduced and oxidised form. J Mol Biol. 2008; 375(3):604–11. PMID: 18061205

45. Garcia-Saez I, Hopkins J, Papamicael C, Franceschini N, Amicosante G, Rossolini GM, et al. The 1.5-A structure of Chryseobacterium meningosepticum zinc beta-lactamase in complex with the inhibitor, D-captopril. J Biol Chem. 2003; 278(26):23868–73. PMID: 12684522.

46. Concha NO, Rasmussen BA, Bush K, Herzberg O. Crystal structure of the wide-spectrum binuclear zinc beta-lactamase from Bacteroides fragilis. Structure. 1996; 4(7):823–36. PMID: 8805566.

47. Yamaguchi Y, Takashio N, Wachino J, Yamagata Y, Arakawa Y, Matsuda K, et al. Structure of metallo-beta-lactamase IND-7 from a Chryseobacterium indologenes clinical isolate at 1.65-A resolution. J Biochem. 2010; 147(6):905–15. doi: 10.1093/jb/mvq029 PMID: 20305272

48. Borra PS, Samuelsen O, Spencer J, Walsh TR, Lorentzen MS, Leiros HK. Crystal structures of Pseudomonas aeruginosa GIM-1: active-site plasticity in metallo-beta-lactamases. Antimicrob Agents Chemother. 2013; 57(2):848–54. Epub 2012/12/05. doi: 10.1128/aac.02227-12 PMID: 23208706; PubMed Central PMCID: PMCPMC3553699.

49. Brown NG, Horton LB, Huang W, Vongpunsawad S, Palzkill T. Analysis of the functional contributions of Asn233 in metallo-beta-lactamase IMP-1. Antimicrob Agents Chemother. 2011; 55(12):5696–702. doi: 10.1128/AAC.00340-11 PMID: 21896903; PubMed Central PMCID: PMC3232802.

50. McNicholas S, Potterton E, Wilson KS, Noble ME. Presenting your structures: the CCP4mg molecular-graphics software. Acta Crystallogr D Biol Crystallogr. 2011; 67(Pt 4):386–94. doi: 10.1107/S0907444911007281 PMID: 21460457; PubMed Central PMCID: PMC3069754.

51. Badarau A, Page MI. Loss of enzyme activity during turnover of the Bacillus cereus beta-lactamase catalysed hydrolysis of beta-lactams due to loss of zinc ion. Journal of biological inorganic chemistry: JBIC: a publication of the Society of Biological Inorganic Chemistry. 2008; 13(6):919–28. doi: 10.1007/s00775-008-0379-2 PMID: 18449576.

52. Gonzalez JM, Meini MR, Tomatis PE, Medrano Martin FJ, Cricco JA, Vila AJ. Metallo-beta-lactamases withstand low Zn(II) conditions by tuning metal-ligand interactions. Nat Chem Biol. 2012; 8(8):698–700. doi: 10.1038/nchembio.1005 PMID: 22729148; PubMed Central PMCID: PMC3470787.

53. Wang Z, Fast W, Benkovic SJ. On the mechanism of the metallo-beta-lactamase from Bacteroides fragilis. Biochemistry. 1999; 38(31):10013–23. PMID: 10433708.

54. King D, Strynadka N. Crystal structure of New Delhi metallo-beta-lactamase reveals molecular basis for antibiotic resistance. Protein Sci. 2011; 20(9):1484–91. doi: 10.1002/pro.697 PMID: 21774017; PubMed Central PMCID: PMC3190144.

55. Ullah JH, Walsh TR, Taylor IA, Emery DC, Verma CS, Gamblin SJ, et al. The crystal structure of the L1 metallo-beta-lactamase from Stenotrophomonas maltophilia at 1.7 A resolution. J Mol Biol. 1998; 284 (1):125–36. PMID: 9811546.

56. Addison AW, Rao TN, Reedijk J, Vanrijn J, Verschoor GC. Synthesis, Structure, and Spectroscopic Properties of Copper(Ii) Compounds Containing Nitrogen Sulfur Donor Ligands—the Crystal and Molecular-Structure of Aqua[1,7-Bis(N-Methylbenzimidazol-2'-Yl)-2,6-Dithiaheptane]Copper(Ii) Perchlorate. J Chem Soc Dalton. 1984;(7:):1349–56. doi: 10.1039/Dt9840001349 WOS: A1984TA65500013.

57. Davies AM, Rasia RM, Vila AJ, Sutton BJ, Fabiane SM. Effect of pH on the active site of an Arg121Cys mutant of the metallo-beta-lactamase from Bacillus cereus: implications for the enzyme mechanism. Biochemistry. 2005; 44(12):4841–9. PMID: 15779910.

58. Karsisiotis AI, Damblon CF, Roberts GC. A variety of roles for versatile zinc in metallo-beta-lactamases. Metallomics: integrated biometal science. 2014; 6(7):1181–97. doi: 10.1039/c4mt00066h PMID: 24696003.

59. Bicknell R, Schaffer A, Waley SG, Auld DS. Changes in the coordination geometry of the active-site metal during catalysis of benzylpenicillin hydrolysis by Bacillus cereus beta-lactamase II. Biochemistry. 1986; 25(22):7208–15. PMID: 3099831.

60. Garrity JD, Bennett B, Crowder MW. Direct evidence that the reaction intermediate of metallo-beta-lactamase L1 is metal bound. Biochemistry. 2005; 44(3):1078–87. PMID: 15654764.

61. Yang H, Aitha M, Marts AR, Hetrick AM, Bennett B, Crowder MW, et al. Spectroscopic and Mechanistic Studies of Heterodimetallic Forms of Metallo-ss-Lactamase NDM-1. J Am Chem Soc. 2014. doi: 10.1021/ja410376s PMID: 24754678.

62. Materon IC, Palzkill T. Identification of residues critical for metallo-beta-lactamase function by codon randomization and selection. Protein Sci. 2001; 10(12):2556–65. PMID: 11714924.

63. Yanchak MP, Taylor RA, Crowder MW. Mutational analysis of metallo-beta-lactamase CcrA from Bacteroides fragilis. Biochemistry. 2000; 39(37):11330–9. PMID: 10985778.